Nuclear Physics A364 (1981) 270–284

STUDY OF π^+ AND π^- ELASTIC SCATTERING FROM ^{40}Ca AND ^{48}Ca IN THE REGION OF THE πN(3, 3) RESONANCE

P. GRETILLAT*, J.-P. EGGER, J.-F. GERMOND, C. LUNKE and E. SCHWARZ

Institut de Physique, Université de Neuchâtel, CH-2000 Neuchâtel, Switzerland

C. PERRIN

ISN, Université de Grenoble, F-38026 Grenoble, France

and

B.M. PREEDOM

University of South Carolina, Columbia SC 29208, USA

Received 8 December 1980

Abstract: Angular distributions for elastic scattering from ^{40}Ca and ^{48}Ca with π^+ and π^- beams were measured at 130, 180 and 230 MeV. A neutron–proton rms radius difference in ^{48}Ca of 0.20 ± 0.05 fm was obtained at 180 MeV within the eikonal framework.

E

NUCLEAR REACTIONS ^{40,48}Ca(π^+, π^+), (π^-, π^-), E = 130, 180, 230 MeV; measured $\sigma(\theta)$. ^{48}Ca deduced neutron, proton rms radius difference in Black disc analysis, eikonal framework.

1. Introduction

In general a study of nuclei starts with a description of nuclear sizes and densities. A basic requirement of even the most simple nuclear model is that it reproduces both the proton and neutron density distributions reasonably well. Electron scattering has provided the most precise measurements of proton and charge density distributions, since high-precision data are available and the elementary interaction is well known. However, in order to gain some knowledge of neutron distributions, hadronic probes must be used. With the advent of high-resolution pion channels and spectrometers at the "meson facilities" it is now possible to gather accurate pion–nucleus scattering data in the energy region of the first pion–nucleus resonance corresponding to an incident pion energy around 180 MeV. One of the primary hopes of these experiments is to take advantage of the strong π^-–neutron interaction at these energies to extract information on neutron distributions by comparison of π^+ and π^- elastic scattering.

* In partial fulfilment of the requirements for the degree "Dr ès Sciences" of the University of Neuchâtel.

In this article, we present a study of elastic scattering from ^{40}Ca and ^{48}Ca with π^+ and π^- beams at 130, 180 and 230 MeV. The calcium isotopes are particularly interesting because extensive theoretical calculations of their nuclear structure exist [1]). In addition, ^{40}Ca is the heaviest stable $N = Z$ nucleus. This allows the investigation of electromagnetic effects without large contributions from the neutron–proton density differences. The comparison with ^{48}Ca should allow the determination of the effect of the eight additional neutrons which close the $f_{7/2}$ shell.

2. Experimental procedure

The experiment was carried out at the Swiss Institute for Nuclear Research (SIN) at Villigen with the πM1 beam and pion spectrometer. The general layout of the experiment is presented in fig. 1. Pions are produced in a 3 mm Be target (B) by a 590 MeV proton beam and enter the πM1 beam at a production angle of 22.5°. The beam consists of two 75° bending magnets (D_1 and D_2), a set of SIN standard quadrupoles (Q_1–Q_9) and an electrostatic separator (crossed fields, Sep and D_S) for removal of protons in the π^+ beam. The accepted momentum range of the incident pions is $\Delta p/p = \pm 1.4\%$. The beam is dispersed in momentum (dispersion =

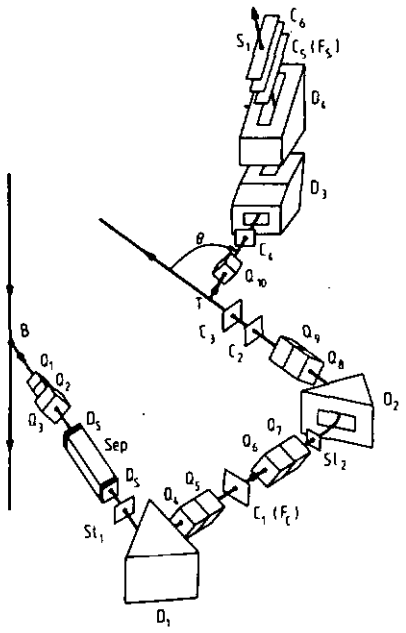

Fig. 1. General layout of the πM1 beam line and pion spectrometer at the Swiss Institute for Nuclear Research (SIN). B = pion production target, D = dipole bending magnet, Q = quadrupole magnet, Sep = electrostatic separator, D_S = dipole magnet of separator, SI = adjustable collimator, C = multi-wire proportional chamber, F_C and F_S = focal plane of channel and spectrometer, T = scattering target, S = scintillator, θ = laboratory scattering angle.

7 cm/% $\Delta p/p$) at the intermediate focal plane (F_C) where each particle is detected by a 20 cm × 7 cm multi-wire proportional chamber (MWPC, C_1) with 1 mm wire spacing and fast digital readout in the x-direction [2]). Farther downstream the dispersed beam is recombined onto an achromatic focus at the location of the scattering target with a spot size of 0.9 cm × 0.7 cm FWHM. Two other 10 cm × 10 cm MWPC (C_2 and C_3) with 1 mm wire spacing and x, y readout 80 cm and 40 cm upstream from the scattering target measure the angle incident on target: The incident beam particles are counted by a coincidence between the 50 MHz r.f. signal and the high voltage planes of the two MWPC C_1 and C_2. Two scintillators downstream from the target allow for a clean beam sampling by using the r.f. signal as a start for a time-of-flight measurement over 20 m in order to account for muons and electrons in the beam. Pion intensities in the experiment with a primary proton beam of ~50 μA were between 1 and 4×10^6 π^+/s and between 2 and 8×10^5 π^-/s incident on a 350 mg·cm^{-2} natural (97%) calcium target and on a 256 mg·cm^{-2} 98% isotopically enriched ^{48}Ca target. The dimensions of the ^{48}Ca target were 15 × 15 mm which is somewhat smaller than the beam spot especially when the target is set at one-half of the spectrometer angle in transmission geometry. Therefore two scintillators were positioned 30 cm vertically below the scattering target in order to provide the relative normalization as a function of target angle. In addition, the beam profile on target was monitored continuously with chambers C_2 and C_3.

The pion spectrometer is of the QDD type with a large solid angle (16 msr), a broad momentum acceptance (±18% $\Delta p/p$) and a momentum resolution of 10^{-3} $\Delta p/p$ FWHM. The scattered particles are detected after the quadrupole Q_{10} by a 20 cm × 20 cm MWPC (C_4) with 1 mm wire spacing and x, y readout and at the end of the spectrometer by two 200 cm × 20 cm MWPC (C_5 and C_6) with three wire planes with 2 mm wire spacing each. Wire plane 1 is used for x-readout whereas wire planes 2 and 3 have their wires set at angles of +30° and −30° with respect to plane 1 giving a y-readout without needing 2 m long wires. The first of the 2 m chambers (C_5) is located close to the focal plane, the second (C_6) parallel to it but 30 cm downstream. In addition, a scintillator (S_1) behind the last MWPC gives the trigger signal for an event. The focal plane is inclined by an average of 55° with respect to the particle trajectories with a dispersion of 55 mm/(% $\Delta p/p$). Muons from π-decay in the spectrometer were largely rejected by imposing ion optical conditions on each particle trajectory. The over-all energy resolution was 500 keV FWHM which is sufficient to separate the elastic scattering peak. The angular resolution amounted to 1° FWHM. More details of the channel, the spectrometer and the experimental set-up are given elsewhere [3]).

3. Data reduction

The angular distributions are presented in figs. 2 and 3. Measurements were carried out at three incident pion energies in the region of the πN(3, 3) resonance:

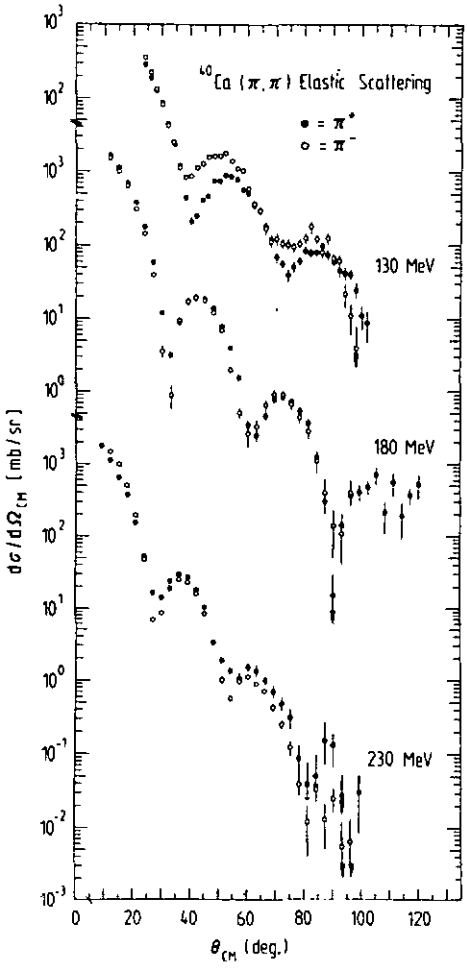

Fig. 2. Comparison of π^+ and π^- – ^{40}Ca c.m. elastic scattering differential cross sections at 130, 180 and 230 MeV versus the pion scattering angle in the c.m.s.

130, 180 and 230 MeV. Except for target contamination, no subtraction of background was required. Our calcium targets contained hydrogen, oxygen and carbon as contaminants. Since the hydrogen kinematics differ significantly from the calcium kinematics, the two elastic peaks are always well separated. Oxygen and carbon contamination is important in the minima of the angular distributions, especially at 180 MeV where the minima are deep. However, beyond the first minimum, our energy resolution is sufficient to separate the contaminants. In the vicinity of the first minima where the elastic calcium peak could not be fully resolved, we were able to decompose the observed larger peak into its constituents by imposing a standard peak shape and a constant target contamination in function of scattering angle using the known elastic pion–oxygen and pion–carbon cross sections [4]). Error bars are

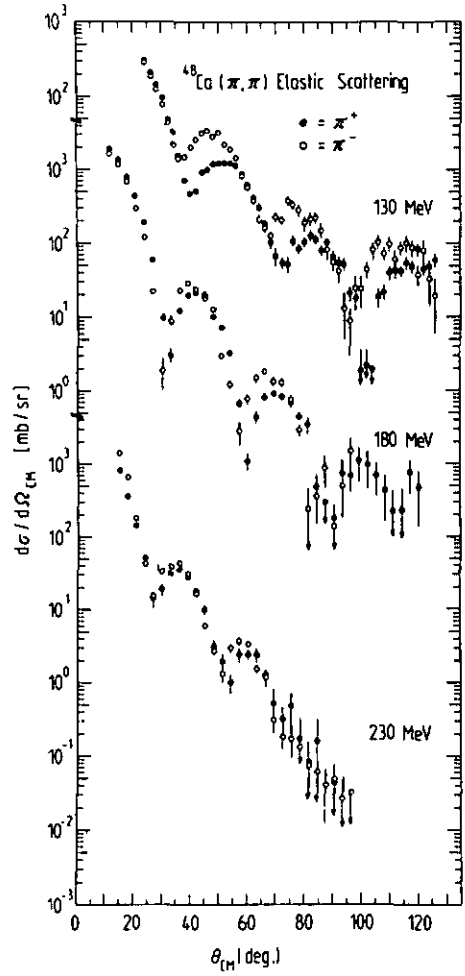

Fig. 3. Comparison of π^+ and π^- – ^{48}Ca c.m. scattering differential cross sections at 130, 180 and 230 MeV versus the pion scattering angle in the c.m.s.

statistical but include the target contaminant subtraction where necessary. The pion spectrometer has an angular acceptance of ~9° FWHM. For one spectrometer position, the data were therefore divided into 3 angular bins of 3° each except at 130 MeV where 4 angular bins of 2° were chosen. Measurements were taken at 6° intervals, thus giving overlapping bins. The relative differences of two bins at the same scattering angle for two spectrometer positions were compatible with statistics. The cross section values were corrected for finite angular resolution by a method similar to the one used by ref. [5]). The beam sampling method gave the relative normalization between π^+ and π^- data, taking beam composition into account. The absolute normalization was obtained by gathering data with a polyethylene $[(CH_2)_n]$ target and scaling it against the known hydrogen cross section [6]). The absolute

TABLE 1

Differential cross section values (in mb/sr) in the c.m.s. versus the c.m. scattering angle for π^+ and π^- elastic scattering off ^{40}Ca and ^{48}Ca at three incident pion energies: 130, 180 and 230 MeV

$\theta_{c.m.}$ (deg.)	$\pi^+ \rightarrow {}^{40}$Ca $\left(\frac{d\sigma}{d\Omega}\right)_{c.m.}$	error	$\pi^- \rightarrow {}^{40}$Ca $\left(\frac{d\sigma}{d\Omega}\right)_{c.m.}$	error	$\theta_{c.m.}$ (deg.)	$\pi^+ \rightarrow {}^{48}$Ca $\left(\frac{d\sigma}{d\Omega}\right)_{c.m.}$	error	$\pi^- \rightarrow {}^{48}$Ca $\left(\frac{d\sigma}{d\Omega}\right)_{c.m.}$	error
				$T_\pi = 130$ MeV					
24.17	293.1	6.12	361.2	10.36	24.14	307.6	4.75	289.8	7.12
26.18	188.5	4.44	229.0	7.70	26.15	215.7	3.76	190.9	5.34
28.19	127.4	3.56	137.2	5.83	28.16	151.4	3.17	126.7	4.35
30.21	88.3	2.57	87.50	3.16	30.17	98.97	1.88	79.27	2.38
32.22	46.1	2.67	43.86	2.67	32.18	59.49	1.88	46.13	2.28
34.23	23.91	1.88	25.69	2.08	34.19	34.06	1.49	22.57	1.58
36.24	12.65	0.79	11.76	0.89	36.20	16.74	0.69	14.66	0.99
38.25	4.50	0.48	8.60	0.80	38.21	7.32	0.53	15.55	1.39
40.27	2.16	0.34	9.09	0.82	40.22	4.88	0.44	20.71	1.59
42.28	2.54	0.25	11.87	0.79	42.23	5.25	0.32	26.26	1.19
44.29	4.17	0.37	13.26	1.09	44.24	9.38	0.55	32.12	1.49
46.30	4.80	0.39	16.24	1.19	46.25	10.31	0.56	35.11	1.59
48.31	7.84	0.44	16.64	0.99	48.26	12.20	0.46	29.46	1.29
50.32	7.76	0.64	16.55	1.29	50.26	12.70	0.59	33.64	2.28
52.33	9.21	0.70	18.24	1.39	52.27	12.90	0.61	23.72	1.89
54.33	8.76	0.51	14.28	0.89	54.28	12.61	0.49	19.76	1.09
56.34	8.11	0.64	11.51	0.89	56.29	11.82	0.66	15.00	1.19
58.35	5.71	0.54	10.62	0.89	58.29	8.76	0.57	8.22	0.855
60.36	5.18	0.31	6.01	0.44	60.30	6.38	0.36	5.87	0.497
62.36	3.56	0.29	3.68	0.41	62.30	4.28	0.37	3.94	0.497
64.37	2.89	0.26	3.01	0.37	64.31	3.22	0.32	2.17	0.368
66.38	1.90	0.16	1.75	0.22	66.31	1.86	0.21	1.61	0.249
68.38	1.27	0.16	1.17	0.24	68.32	1.015	0.21	1.32	0.319
70.39	0.707	0.119	1.24	0.26	70.32	0.697	0.18	2.30	0.428
72.39	0.568	0.080	1.05	0.16	72.33	0.548	0.110	2.09	0.329
74.40	0.398	0.090	1.03	0.18	74.33	0.528	0.130	3.87	0.608
76.40	0.508	0.100	0.97	0.18	76.33	1.107	0.190	3.39	0.568
78.40	0.618	0.090	1.08	0.16	78.34	0.858	0.120	2.83	0.499
80.41	0.858	0.130	1.28	0.26	80.34	1.078	0.180	1.856	0.439
82.41	0.798	0.130	1.80	0.31	82.34	1.318	0.210	2.166	0.469
84.41	0.809	0.090	1.26	0.16	84.34	1.169	0.130	2.237	0.320
86.41	0.999	0.130	0.819	0.160	86.34	0.809	0.130	1.549	0.320
88.41	0.760	0.120	1.280	0.200	88.34	1.050	0.150	0.840	0.240
90.41	0.600	0.080	0.670	0.110	90.34	0.680	0.090	0.570	0.130
92.41	0.460	0.090	0.620	0.140	92.34	0.550	0.110	0.420	0.130
94.41	0.420	0.090	0.220	0.080	94.34	0.531	0.110	0.130	0.080
96.41	0.411	0.060	0.110	0.050	96.34	0.210	0.050	0.080	0.050
98.41	0.251	0.060	0.040	0.040	98.34	0.180	0.060	0.250	0.120
100.41	0.110	0.040	≤0.040		100.34	0.019	0.019	0.251	0.120
102.40	0.088	0.041	≤0.040		102.34	0.022	0.015	0.441	0.130
					104.33	≤0.020		0.832	0.221
					106.33	0.191	0.060	1.074	0.251
					108.33	0.221	0.050	0.723	0.161

TABLE 1 (continued)

$\theta_{c.m.}$ (deg.)	$\pi^+ \rightarrow {}^{40}Ca$ $\left(\frac{d\sigma}{d\Omega}\right)_{c.m.}$	error	$\pi^- \rightarrow {}^{40}Ca$ $\left(\frac{d\sigma}{d\Omega}\right)_{c.m.}$	error	$\theta_{c.m.}$ (deg.)	$\pi^+ \rightarrow {}^{48}Ca$ $\left(\frac{d\sigma}{d\Omega}\right)_{c.m.}$	error	$\pi^- \rightarrow {}^{48}Ca$ $\left(\frac{d\sigma}{d\Omega}\right)_{c.m.}$	error
				$T_\pi = 130$ MeV					
					110.32	0.402	0.090	0.994	0.251
					112.32	0.432	0.101	0.603	0.201
					114.31	0.432	0.070	0.894	0.191
					116.31	0.553	0.111	1.025	0.271
					118.30	0.493	0.101	0.885	0.241
					120.30	0.765	0.101	0.382	0.121
					122.29	0.463	0.101	0.795	0.302
					124.29	0.483	0.101	0.332	0.191
					126.28	0.604	0.121	0.201	0.141
				$T_\pi = 180$ MeV					
12.10	1684	23.6	1579	28.4	12.08	2017	31.1	1859	46.4
15.13	1168	25.6	1034	20.6	15.11	1433	23.6	1210	36.5
18.15	703	10.3	653	13.6	18.13	834	10.9	704	15.0
21.18	386	6.59	313	8.55	21.15	466	8.70	302	10.9
24.20	181	3.94	145	4.08	24.17	193	3.79	110.6	4.54
27.22	59.2	1.87	40.0	1.95	27.19	62.3	2.74	22.3	2.67
30.25	12.3	0.91	3.62	0.78	30.20	9.83	1.00	1.88	0.94
33.27	3.24	0.47	0.935	0.43	33.22	3.15	0.80	8.91	1.29
36.29	8.92	0.59	9.43	0.55	36.24	12.6	0.87	23.6	0.99
39.31	17.1	0.59	17.8	0.80	39.26	20.2	1.00	28.7	1.48
42.33	20.4	0.69	20.1	0.78	42.27	23.1	0.50	24.2	0.89
45.35	19.1	0.69	19.1	0.86	45.29	20.3	0.50	17.9	0.79
48.36	14.2	0.494	12.6	0.55	48.30	12.6	0.30	10.30	0.495
51.38	8.09	0.396	7.04	0.38	51.32	7.31	0.52	3.043	0.307
54.40	4.14	0.228	2.01	0.19	54.33	3.37	0.22	1.230	0.149
57.41	1.58	0.129	0.515	0.078	57.34	0.670	0.106	0.285	0.100
60.42	0.349	0.069	0.271	0.102	60.35	0.111	0.031	0.789	0.127
63.44	0.252	0.050	0.339	0.077	63.36	0.447	0.094	1.540	0.268
66.45	0.473	0.069	0.665	0.127	66.37	0.831	0.099	1.829	0.219
69.46	0.797	0.089	0.942	0.157	69.38	0.928	0.139	1.373	0.229
72.47	0.842	0.090	0.872	0.157	72.39	0.853	0.088	1.314	0.169
75.47	0.734	0.080	0.684	0.126	75.39	0.702	0.093	0.760	0.152
78.48	0.538	0.080	0.454	0.087	78.40	0.456	0.065	0.287	0.089
81.48	0.369	0.060	0.288	0.061	81.40	0.356	0.091	0.024	0.024
84.49	0.122	0.030	0.114	0.037	84.41	0.049	0.024	0.036	0.021
87.49	0.030	0.010	0.040	0.021	87.41	≤0.030		0.091	0.046
90.49	0.0015	0.0015	0.014	0.009	90.41	≤0.018		0.014	0.014
93.49	0.014	0.006	0.011	0.007	93.41	0.074	0.043	0.053	0.035
96.49	0.036	0.010	0.040	0.020	96.41	0.059	0.030	0.159	0.071
99.48	0.041	0.010			99.40	0.110	0.056		
102.48	0.048	0.010			102.40	0.097	0.057		
105.47	0.071	0.020			105.39	0.072	0.035		
108.46	0.021	0.010			108.39	0.043	0.027		

TABLE 1 (continued)

$\theta_{c.m.}$ (deg.)	$\pi^+ \rightarrow {}^{40}Ca$ $\left(\frac{d\sigma}{d\Omega}\right)_{c.m.}$	error	$\pi^- \rightarrow {}^{40}Ca$ $\left(\frac{d\sigma}{d\Omega}\right)_{c.m.}$	error	$\theta_{c.m.}$ (deg.)	$\pi^+ \rightarrow {}^{48}Ca$ $\left(\frac{d\sigma}{d\Omega}\right)_{c.m.}$	error	$\pi^- \rightarrow {}^{48}Ca$ $\left(\frac{d\sigma}{d\Omega}\right)_{c.m.}$	error
				$T_\pi = 180$ MeV					
111.46	0.056	0.020			111.38	0.022	0.022		
114.45	0.019	0.010			114.37	0.023	0.023		
117.43	0.037	0.010			117.36	0.077	0.039		
120.42	0.053	0.020			120.35	0.047	0.033		
				$T_\pi = 230$ MeV					
9.09	1779	167.3							
12.12	1135	41.8	1511	60.5					
15.15	657	29.8	995	17.4	15.12	639	39.4	1523	152
18.18	363.4	11.1	507	7.60	18.15	364	18.8	668	26.9
21.20	154.2	7.15	196.2	5.27	21.17	121.3	14.0	177	13.3
24.23	53.6	3.22	48.7	2.72	24.19	51.7	6.99	42.1	4.13
27.26	16.7	1.74	6.95	1.01	27.21	14.5	4.58	15.7	2.58
30.28	13.9	1.23	8.78	0.74	30.24	18.8	3.18	33.6	2.19
33.31	23.9	1.43	19.0	0.85	33.26	31.6	2.76	38.8	2.19
36.33	29.4	1.33	25.0	0.67	36.28	35.2	2.29	43.9	1.86
39.36	26.8	1.74	23.3	0.77	39.30	29.5	2.55	31.2	2.03
42.38	18.2	1.015	16.1	0.58	42.32	17.6	0.79	16.5	0.828
45.40	10.7	0.81	8.57	0.49	45.33	9.86	1.47	5.95	0.575
48.42	3.38	0.295	3.35	0.19	48.35	3.23	0.66	2.72	0.355
51.44	1.88	0.254	1.007	0.105	51.37	1.95	0.62	1.30	0.333
54.46	1.357	0.179	0.573	0.058	54.38	1.014	0.315	3.05	0.340
57.47	1.050	0.206	0.985	0.100	57.40	2.45	0.618	3.70	0.424
60.49	1.524	0.197	1.127	0.084	60.41	2.45	0.448	3.41	0.322
63.50	1.371	0.239	0.893	0.094	63.42	2.41	0.555	1.55	0.260
66.52	1.000	0.139	0.711	0.066	66.43	1.20	0.333	1.19	0.168
69.53	0.716	0.156	0.431	0.063	69.44	0.522	0.301	0.303	0.100
72.54	0.476	0.097	0.252	0.035	72.45	0.321	0.160	0.189	0.063
75.55	0.307	0.098	0.121	0.030	75.46	0.484	0.242	0.170	0.077
78.55	0.087	0.044	0.039	0.012	78.46	0.169	1.169	0.136	0.056
81.56	0.039	0.039	0.012	0.0085	81.47	≤0.075		0.075	0.055
84.56	0.050	0.050	0.033	0.012	84.47	0.163	0.163	0.061	0.036
87.56	0.152	0.077	0.013	0.0085	87.47			0.039	0.027
90.56	0.132	0.067	0.025	0.0093	90.47	≤0.043		0.048	0.027
93.56	0.027	0.027	0.0055	0.0055				0.026	0.026
96.56			0.0065	0.0065				≤0.032	
99.56	0.030	0.022							

normalization error was estimated at ±10% for ^{40}Ca. Since the ^{48}Ca target is reduced in size, a polyethylene target of this smaller size was also used. However, we estimate the ^{48}Ca normalization error at ±15% because of the sensitivity of target positioning.

Table 1 gives the measured elastic cross section values in the c.m. system. The 130 MeV data were previously published in ref. [7]).

4. Black disk analysis

Although the black disk model is a very crude analysis, it can be justified by the fact that the nucleus in the region of the πN(3, 3) resonance is strongly absorbing for pions. Therefore, information on neutron distributions in nuclei is obtained because of rather than in spite of the blackness of the nucleus to pions in this energy range. However, neutron radii obtained with a black disk analysis will be realistic only in the tail of the nucleus since pion–nucleus scattering in our case is a surface phenomenon. In particular, the black disk radii R will be energy dependent and certainly much larger than the usual half-density or rms radii. In the black disk limit, the elastic scattering amplitude is given by

$$f(q) = ikR^2 \frac{J_1(qR)}{qR}, \tag{4.1}$$

where $q = 2k \sin \frac{1}{2}\theta$ is the momentum transfer, θ the c.m. scattering angle, R the black disk radius, J_1 the Bessel function of the first kind and order 1, k the pion wave number.

If the analysis is limited to the angular region around the first diffraction minimum, the only experimental information that enters into this model is the position of this first minimum where $J_1(q_1R) = 0$ for $q_1R = 3.83$. In order to determine precisely this position, the angular distributions were fitted using a phenomenological scattering amplitude given by [20])

$$F(q) = F(0)\left[\prod_{i=1}^{4}\left(1 - \frac{q^2}{q_i^2}\right)\right] e^{-\alpha q^2/2}, \tag{4.2}$$

where q_i^2 denote the complex zeros and α is the slope parameter taken to be real. In contrast to the analysis of our ^{12}C data [4b]) all Coulomb effects were neglected in these fits mainly because their inclusion would have required precise total cross section measurements. Table 2 shows the phenomenological fit parameters Re q_1^2 and Im q_1^2 together with the χ^2 per degree of freedom. It should be noted that equation (4.2) was also used for correcting the data for finite angular resolution [see refs. [4a,5])].

The black disk radius R is then related to the first complex zero q_1^2 by

$$R = 3.83\sqrt{\mathrm{Re}\left(\frac{1}{q_1^2}\right)}. \tag{4.3}$$

The results deduced from the values shown in table 2 are presented in table 3. It should be noted that black disk radii for the 130 MeV results which were published earlier [7]) have changed slightly because the position of the first minimum is now determined more accurately with our fitting procedure.

If we assume that all Coulomb effects in $\Delta R_{48} = R(\pi^-, 48) - R(\pi^+, 48)$ are the same as those in $\Delta R_{40} = R(\pi^-, 40) - R(\pi^+, 40)$, then the quantity

$$\Delta x = \Delta R_{48} - \Delta R_{40} \tag{4.4}$$

TABLE 2

Parameters Re (q_1^2) and Im (q_1^2) deduced by fitting the formula $f(\theta) = f(0)[\prod_{i=1}^{4}(1 - q^2/q_i^2)]\exp(-\frac{1}{2}aq^2)$ to the elastic data at 130, 180 and 230 MeV separately for π^+ and π^- in the c.m.s., together with the χ^2 per degree of freedom (χ^2/N)

Energy (MeV)	Pion	Nucleus	Re q_1^2 (fm^{-2})	Im q_1^2 (fm^{-2})	χ^2/N
130	π^+	^{40}Ca	0.647 ± 0.003	0.0806 ± 0.0036	1.35
130	π^-	^{40}Ca	0.564 ± 0.003	0.1101 ± 0.0035	1.21
130	π^+	^{48}Ca	0.629 ± 0.002	0.1115 ± 0.0027	1.43
130	π^-	^{48}Ca	0.502 ± 0.002	0.1240 ± 0.0031	2.20
180	π^+	^{40}Ca	0.664 ± 0.002	0.0653 ± 0.0048	0.78
180	π^-	^{40}Ca	0.637 ± 0.002	0.00001 ± 0.0111	1.91
180	π^+	^{48}Ca	0.647 ± 0.002	0.0548 ± 0.0066	1.18
180	π^-	^{48}Ca	0.567 ± 0.003	0.0347 ± 0.0108	1.40
230	π^+	^{40}Ca	0.677 ± 0.005	0.1523 ± 0.0067	1.67
230	π^-	^{40}Ca	0.703 ± 0.003	0.0769 ± 0.0063	1.38
230	π^+	^{48}Ca	0.646 ± 0.009	0.1583 ± 0.0133	1.12
230	π^-	^{48}Ca	0.620 ± 0.005	0.0868 ± 0.0076	2.55

will be a direct measure of the effect of the eight additional neutrons in ^{48}Ca. To lowest order Δx is related to the neutron excess [21]) by

$$\Delta x = \left(a\frac{\Delta\rho}{\rho}\right)_{^{48}\mathrm{Ca}} - \left(a\frac{\Delta\rho}{\rho}\right)_{^{40}\mathrm{Ca}}, \tag{4.5}$$

where $\Delta\rho = \rho_n - \rho_p$ and $\rho = \rho_n + \rho_p$ are evaluated at the average black disk radius. The parameter a corresponds to the diffuseness of the optical potential [9]) which is larger than the nuclear diffuseness because of the folding with the πN interaction. On the basis of a first-order optical potential calculation, we estimate it to be 0.13 fm larger and energy independent. Values deduced from eq. (4.5) using Negele's DME

TABLE 3

Black disk analysis results for π^+ and π^- at 130, 180 and 230 MeV for both ^{40}Ca and ^{48}Ca

T_π (MeV)	^{40}Ca			^{48}Ca			$\Delta x = \Delta R_{48} - \Delta R_{40}$ (fm)	Δx_{th} (fm)
	$R(\pi^-)$ (fm)	$R(\pi^+)$ (fm)	ΔR_{40} (fm)	$R(\pi^-)$ (fm)	$R(\pi^+)$ (fm)	ΔR_{48} (fm)		
130	5.00	4.72	0.28	5.25	4.75	0.50	0.22	0.215
180	4.80	4.68	0.12	5.08	4.75	0.33	0.21	0.205
230	4.54	4.54	0.00	4.82	4.63	0.19	0.19	0.191

Errors are 0.05 fm. In addition, values deduced from eq. (4.5) using Negele's DME densities as input [1a]) are shown under Δx_{th}.

densities as input [1a]) are also shown as $\Delta x_{\rm th}$ in table 3. They are in excellent agreement with the values deduced from our data. Note that if there were no neutron–proton radius difference, eq. (4.5) would reduce to $\Delta x = a(N-Z)/A$ with $A = 48$.

5. Improved black disk analysis

Starting from the eikonal approximation, an analytical expression can be obtained for the scattering amplitude. Such a scheme has recently been explored by Bethe and Johnson [8]). Their result was very simple but it did not include the Coulomb effects and did not describe accurately the magnitude of the cross section at the position of the first secondary maximum. An improved calculation was carried out by Germond and Johnson [9]) based on techniques developed many years ago by Frahn and Venter [10]). Germond and Johnson characterize the scattering amplitude by three numbers: a radius parameter b_1, a diffuseness type parameter a and a parameter Y related to the depth of the diffraction minimum. For the strong interaction part, the result obtained is of the fuzzy black disk type [11]) whereas when Coulomb is included the usual Bethe phase [12]) is present but in addition the trajectory and energy shift effects will be included through b_1, a and Y and in the dependence of the scattering amplitude on them.[20]). Furthermore, the parameter Y is very small at 180 MeV since the first diffraction minima are deep. Defining Δc as the neutron half-density radius difference between ^{48}Ca and ^{40}Ca and assuming a Fermi-type distribution

$$\rho(r) = \rho(0)\frac{1}{1+e^{(r-c)/z}} \tag{5.1}$$

equations relating Δc to b_1 and a can be obtained [9]):

$$\Delta b_1(\pi^+) = b_1^{48}(\pi^+) - b_1^{40}(\pi^+) \approx a \log\left\{1+\frac{1}{2A}\left[\Delta N + (\tfrac{1}{2}A + \Delta N)\frac{\partial b_1}{\partial c}\frac{\Delta c}{a}\right]\right\}, \tag{5.2a}$$

$$\Delta b_1(\pi^-) = b_1^{48}(\pi^-) - b_1^{40}(\pi^-) = a \log\left\{1+\frac{3}{2A}\left[\Delta N + (\tfrac{1}{2}A + \Delta N)\frac{\partial b_1}{\partial c}\frac{\Delta c}{a}\right]\right\}, \tag{5.2b}$$

where $A = 40$, i.e. the nucleon number in ^{40}Ca, and $\Delta N = N - Z = 8$ is the neutron excess in ^{48}Ca. Since the two equations (5.2) above do not contain any difference in diffuseness between ^{48}Ca and ^{40}Ca, we generalized them to include a variation of z (ref. [13])]. The final equations are then

$$\Delta c(\pi^+) = \frac{a[\exp\{\Delta b_1(\pi^+)/a\} - (1+\Delta N/2A)(1+(\partial b_1/\partial z)(\Delta z/a))]}{(\frac{1}{2}+\Delta N/A)\frac{1}{2}\partial b_1/\partial c}, \tag{5.3a}$$

$$\Delta c(\pi^-) = \frac{a[\exp\{\Delta b_1(\pi^-)/a\} - (1+3\Delta N/2A)(1+(\partial b_1/\partial z)(\Delta z/a))]}{(\frac{1}{2}+\Delta N/A)\frac{3}{2}\partial b_1/\partial c}, \tag{5.3b}$$

where Δz is the difference of diffuseness of the Fermi matter distributions of ^{48}Ca and ^{40}Ca. At 180 MeV, $a = 0.65$ fm, $\partial b_1/\partial c = 0.59$ and $\partial b_1/\partial z = 1.78$. These numbers are justified in ref. [9]) on the basis of a first-order optical potential calculation. We fitted our 180 MeV data in the angular range between 15° and 55° which corresponds to the region of the first diffraction minimum. The values obtained for b_1, a and Y are shown in table 4. As expected, Y is small but a is slightly larger than 0.65 fm. We therefore took $a = 0.68$ fm which is the average value of the reference nucleus ^{40}Ca. Equating $\Delta c(\pi^+)$ and $\Delta c(\pi^-)$ results in $\Delta z = -0.012$ fm which is reasonably small and finally with Δz known one obtains $\Delta c(\pi^\pm) = 0.26$ fm which is in good agreement with the theoretical calculations by Lombard [1]), giving $\Delta c_{\text{theor}} = 0.28$ fm and $\Delta z_{\text{theor}} = -0.025$ fm. However, those models also predict $c_p^{48} \neq c_p^{40} \neq c_n^{40}$, whereas we defined them as equal.

It should be noted that in this model pions are sensitive to approximately the one-tenth density radius. Therefore, the determination of the rms radius difference requires an extrapolation which can only be carried out within an analytical form of the density. Using a Fermi distribution leads to an rms radius difference

$$\Delta^{48}_{\text{Ca}} = \langle r^2_{\text{n,rms}} \rangle^{1/2} - \langle r^2_{\text{p,rms}} \rangle^{1/2} = 0.20 \pm 0.05 \text{ fm},$$

where the quoted error includes uncertainties due to the fitting procedure. It is not surprising that this theory works well at 180 MeV where the minima are extremely deep since it is based on a fuzzy black disk formula. However, an extension to lower or higher incident pion energies is significantly more difficult. In fact, using the analytical form of the scattering amplitude proposed in ref [9]), we were unable to get reasonable χ^2 fits to our 130 MeV and 230 MeV data with meaningful values for the parameters, in particular Y. Therefore, we did not try to extract a neutron–proton radius difference from the data at the two energies above within this model.

6. Results, discussion and conclusions

Angular distributions for pion elastic scattering from ^{40}Ca and ^{48}Ca were measured at three pion energies: 130, 180 and 230 MeV. Measurements were carried out for both π^+ and π^- projectiles. Black disk model calculations were done

TABLE 4

Values obtained for b, a and Y for π^+ and π^- scattering off ^{40}Ca and ^{48}Ca at 180 MeV in the angular range $15° \leq \theta \leq 55°$

Isotope	b (fm)	a (fm)	Y
^{40}Ca, π^-	4.689 ± 0.008	0.697 ± 0.008	−0.132 ± 0.034
^{40}Ca, π^+	4.573 ± 0.008	0.668 ± 0.007	−0.120 ± 0.022
^{48}Ca, π^-	4.964 ± 0.011	0.719 ± 0.010	−0.006 ± 0.049
^{48}Ca, π^+	4.665 ± 0.008	0.658 ± 0.006	−0.141 ± 0.024

at all three energies. Furthermore, at 180 MeV, an improved fuzzy black disk type model was used.

The black disk results were shown to be in agreement with Negele's predictions for the neutron–proton density differences in ^{48}Ca compared with ^{40}Ca using a linear relation between ΔR and $\Delta\rho/\rho$. Furthermore, by assuming an over-all error of ± 0.05 fm, the results for the differences at the three energies are compatible although the black disk radius values vary between 4.54 and 5.25 fm (see table 3).

The merit of the analytical theory by Germond and Johnson [9]) is that it enables the extraction of a rms radius difference at 180 MeV assuming a Fermi-type density distribution. Our result of 0.20 ± 0.05 fm for $\Delta^{48}_{Ca} = \langle r^2_{n,rms}\rangle^{1/2} - \langle r^2_{p,rms}\rangle^{1/2}$ is in good agreement with calculated density distributions [1]). However, this number is dependent on the shape assumed for the density and the analysis was impossible at the two other energies.

It is clear that optical-model calculations should be an improved technique to calculate pion–nucleus elastic scattering away from the πN(3, 3) resonance. Such a study was carried out by Sternheim and Yoo [14]) with our 130 MeV data. However, they show that single energy elastic scattering results alone are insufficient to determine neutron density parameters, since changes in the density can be offset by varying the optical-model parameters. In addition, we performed an optical-model calculation on ^{28}Si [ref. [15])] using the computer code FITPI [16]) and fitting the strength and density parameters to the measured angular distributions. Although a satisfactory description of collective excitations in ^{28}Si was obtained via DWIA, the fitted half-density radius parameter needed was 2.5 fm and not 3.1 fm as deduced from electron scattering [17]). We found the same problems when we tried to fit our ^{40}Ca data. Therefore, no reasonable radius could be extracted using FITPI type programs.

Microscopic first-order optical-model calculations were attempted using PIPIT [22]). For ^{40}Ca, it was impossible to obtain results having the correct location of the minima without using unrealistically small values of the half-density radius parameter. Because of this fact, these calculations are not presented here. The same problem existed for ^{48}Ca. However, it should be noted that the additional strength of the $\pi^- + {}^{48}$Ca interaction due to the supplementary eight neutrons resulted in an angular shift of the minima with respect to the $\pi^+ + {}^{48}$Ca angular descriptions. This calculated shift is almost of the same size as the observed shift, indicating that much of the difference in the position of the minima may be due to the difference in effective strength and not to a radius difference. However, until optical-model calculations can be carried out using realistic nuclear density parameters, it will be difficult to extract the effects of differences in interaction strength from differences in nuclear radii.

We believe that the publication of our data, together with the preliminary elastic scattering results from LAMPF at 115 MeV, 180 MeV (compatible with ours), 291 MeV [ref [18])] and recent LAMPF single-charge exchange results [19]) at 180 MeV

should enable an improved optical-model analysis resulting in meaningful radius parameter *differences*.

The authors would like to thank J. Jansen for help in the early stages of the experiment. Also, it is a pleasure to acknowledge useful discussions with H.A. Bethe and M.B. Johnson who started the work on the improved black disk model, and with H. Baer and C. Morris with regard to their experiment. This work was supported in part by the Swiss National Science Foundation and the US National Science Foundation.

References

1a) J.W. Negele, Phys. Rev. C1 (1969) 1260; C9 (1974) 1054;
J.W. Negele and D. Vautherin, Phys. Rev. C5 (1972) 1472; C11 (1975) 1031
1b) M. Beiner, H. Flocard, Nguyen van Giai and P. Quentin, Nucl. Phys. A238 (1975) 29;
M. Beiner and R.J. Lombard, Ann. of Phys. 86 (1974) 262;
R.J. Lombard, private communication
1c) For a general review, J.W. Negele, in Proc. LAMPF Workshop on pion single charge exchange, H. Baer *et al.* ed., LA-7892-C (1979) p. 250
2) R. Foglio, C. Perrin, J. Pouxe, U. Bart and E. Schwarz, Proc. of the 2nd Ispra nuclear electronics Symposium (1975) p. 129
3) J.-P. Albanèse, J. Arvieux, E.T. Boschitz, R. Corfu, J.-P. Egger, P. Gretillat, C.H.Q. Ingram, C. Lunke, E. Pedroni, C. Perrin, J. Piffaretti, L. Pflug, E. Schwarz, C. Wiedner and J. Zichy, Nucl. Instr. 158 (1979) 363
4a) J. Piffaretti, R. Corfu, J.-P. Egger, P. Gretillat, C. Lunke, E. Schwarz, C. Perrin and B.M. Preedom, Phys. Lett. 71B (1977) 324
4b) B. Chabloz, R. Corfu, J.-P. Egger, J.-F. Germond, P. Gretillat, C. Lunke, J. Piffaretti, E. Schwarz, C. Perrin, J.E. Bolger and J. Zichy, Phys. Lett. 81B (1979) 143
4c) J.-P. Albanèse, J. Arvieux, E.T. Boschitz, C.H.Q. Ingram, L. Pflug, C. Wiedner and J. Zichy, Phys. Lett. 73B (1978) 119
5) F. Binon, P. Duteil, J.-P. Garron, J. Gorres, L. Hugon, J.-P. Peigneux, C. Schmit, M. Spighel and J.-P. Stroot, Nucl. Phys. B17 (1970) 168
6) P.J. Bussey, J.R. Carter, D.R. Dance, D.V. Bugg, A.A. Carter and A.M. Smith, Nucl. Phys. B58 (1973) 363
7) J.-P. Egger, R. Corfu, P. Gretillat, C. Lunke, J. Piffaretti, E. Schwarz, C. Perrin, J. Jansen and B.M. Preedom, Phys. Rev. Lett. 39 (1977) 1608
8) M.B. Johnson and H.A. Bethe, Comments Nucl. Part. Phys. 8 (1978) 75
9) J.-F. Germond and M.B. Johnson, Phys. Rev. C22 (1980) 1622
10) W.E. Frahn and R.H. Venter, Ann. of Phys. 24 (1963) 243;
R.H. Venter, Ann. of Phys. 25 (1963) 405
11) E.V. Inopin and Yu.A. Berezhnoy, Nucl. Phys. 63 (1965) 689
12) H.A. Bethe, Ann. of Phys. 3 (1958) 190
13) P. Gretillat, thesis, University of Neuchâtel (1980)
14) M.M. Sternheim and K.-B. Yoo, Phys. Rev. Lett. 41 (1978) 1781
15) B.M. Preedom, R. Corfu, J.-P. Egger, P. Gretillat, C. Lunke, J. Piffaretti, E. Schwarz, J. Jansen and C. Perrin, Nucl. Phys. A326 (1979) 385
16) M.D. Cooper and R.A. Eisenstein, LASL Informal Report LA-5929-MS, April 1975
17) S.W. Brain, A. Johnston, W.A. Gillespie, E.W. Lees and R.P. Singhal, J. of Phys. G3 (1977) 821
18) K.G. Boyer *et al.*, Conf. on meson-nuclear physics, ed. E.V. Hungerford III, AIP Conf. Proc. 54 (1979) 529;
C. Morris, private communication

19) H.W. Baer *et al.*, Int. Conf. on Nucl. Phys. Berkeley (1980); and private communication
20) J.-F. Germond and C. Wilkin, Ann. of Phys. **121** (1979) 285
21) M.B. Johnson in Proc. of the LAMPF Workshop on pion single charge exchange; H. Baer *et al.*, ed., LA-7892-C (1979) p. 343
22) R.A. Eisenstein and F. Tabakin, Comp. Phys. Comm. **12** (1976) 237